

Unbiased Hubble constant estimation from binary neutron star mergers

Daniel J. Mortlock,^{1,2,3,*} Stephen M. Feeney,⁴ Hiranya V. Peiris,^{5,6}
Andrew R. Williamson,^{7,8} and Samaya M. Nissanke^{7,8}

¹*Astrophysics Group, Imperial College London, Blackett Laboratory, Prince Consort Road, London SW7 2AZ, UK*

²*Department of Mathematics, Imperial College London, London SW7 2AZ, UK*

³*Department of Astronomy, Stockholm University, AlbaNova, SE-10691 Stockholm, Sweden*

⁴*Center for Computational Astrophysics, Flatiron Institute, 162 5th Avenue, New York, NY 10010, USA*

⁵*Department of Physics & Astronomy, University College London, Gower Street, London WC1E 6BT, UK*

⁶*Oskar Klein Centre for Cosmoparticle Physics, Stockholm University, AlbaNova, Stockholm SE-106 91, Sweden*

⁷*GRAPPA, Anton Pannekoek Institute for Astronomy and Institute of High-Energy Physics,*

University of Amsterdam, Science Park 904, 1098 XH Amsterdam, The Netherlands

⁸*Nikhef, Science Park 105, 1098 XG Amsterdam, The Netherlands*

Gravitational wave (GW) observations of binary neutron star (BNS) mergers can be used to measure luminosity distances and hence, when coupled with estimates for the mergers' host redshifts, infer the Hubble constant, H_0 . These observations are, however, affected by GW measurement noise, uncertainties in host redshifts and peculiar velocities, and are potentially biased by selection effects and the mis-specification of the cosmological model or the BNS population. The estimation of H_0 from samples of BNS mergers with optical counterparts is tested here by using a phenomenological model for the GW strains that captures both the data-driven event selection and the distance-inclination degeneracy, while being simple enough to facilitate large numbers of simulations. A rigorous Bayesian approach to analyzing the data from such simulated BNS merger samples yields results that are unbiased, have the appropriate uncertainties, and are robust to model mis-specification. Applying such methods to a sample of $N \simeq 50$ BNS merger events, as LIGO+Virgo is expected to produce in the next ~ 5 years, should yield robust and accurate Hubble constant estimates that are precise to a level of $\sim 1 \text{ km s}^{-1} \text{ Mpc}^{-1}$, sufficient to reliably resolve the current tension between local and cosmological measurements of H_0 .

I. INTRODUCTION

The current expansion rate of the Universe is characterized by the Hubble constant, H_0 . While there is broad consensus that $H_0 \simeq 70 \text{ km s}^{-1} \text{ Mpc}^{-1}$, there is a 3.6σ tension between the most recent local and cosmological measurements: the anchor-Cepheid-supernova distance ladder gives $H_0 = 73.5 \pm 1.6 \text{ km s}^{-1} \text{ Mpc}^{-1}$ [1]; while the *Planck* cosmic microwave background (CMB) data, combined with the assumption of a standard flat cold dark matter (Λ CDM) cosmological model, imply that $H_0 = 67.3 \pm 0.6 \text{ km s}^{-1} \text{ Mpc}^{-1}$ [2]. It is tempting to use this tension as motivation for rejecting or extending Λ CDM [3–25], but before settling on such an exciting possibility it is necessary to ensure that the discrepancy is not due to limitations in the analysis of one or both of the datasets [26–39].

The most direct way of resolving this ‘Hubble trouble’ would be an independent local measurement of H_0 , which can be provided by multi-messenger (MM) observations [40, 41] of binary neutron star (BNS) mergers [42–46] and mergers of neutron stars (NSs) and black holes (BHs) [44, 47, 48]. With the advent of Advanced LIGO and Advanced Virgo, it is now possible to detect gravitational waves (GWs) produced during BNS inspirals [49] and, by analyzing the resulting waveforms [50], estimate the luminosity distance to such systems [51].

Coupled with redshift measurements from an electromagnetic (EM) counterpart (e.g., [45–47, 52–54]) (or a set of potential counterparts using a probabilistic host galaxy approach [42, 53, 55–59]), BNS and NS-BH mergers can hence be used to constrain H_0 . The first BNS merger event detected in GWs, GW 170817/GRB 170817A, provided the constraint that $H_0 = 70.0_{-8.0}^{+12.0} \text{ km s}^{-1} \text{ Mpc}^{-1}$ [46]. This was refined to $H_0 = 68.9_{-4.6}^{+4.7} \text{ km s}^{-1} \text{ Mpc}^{-1}$ [60] by using radio observations to obtain better, if model-dependent, constraints on the system inclination [61]. Conversely, if it had been impossible to identify an EM counterpart, the GW measurements alone would have yielded $H_0 = 70.0_{-23.0}^{+48.0} \text{ km s}^{-1} \text{ Mpc}^{-1}$ [58]. A NS-BH merger could provide tighter constraints on H_0 due to the higher mass [44] and the possibility that the BH induces precession of the orbital plane [48]. However, as NS-BH mergers have yet been identified in either GW or EM observations, the focus here is on BNS mergers.

A sample of ~ 50 BNS merger events, which might come in the next ~ 5 years, could yield a measurement of H_0 with a precision of $\sim 1.4 \text{ km s}^{-1} \text{ Mpc}^{-1}$ [53, 54, 62]. This would be sufficient to resolve the current tension [54], but only if the data analysis produces H_0 estimates that have correct uncertainties and that are unbiased. One potential source of bias is selection effects, as detection according to the observed GW signal-to-noise ratio (SNR) will preferentially include events for which the measurement noise has augmented the signal, making such mergers appear to be closer than they are. Unless accounted for, this selection effect would result in

* mortlock@ic.ac.uk

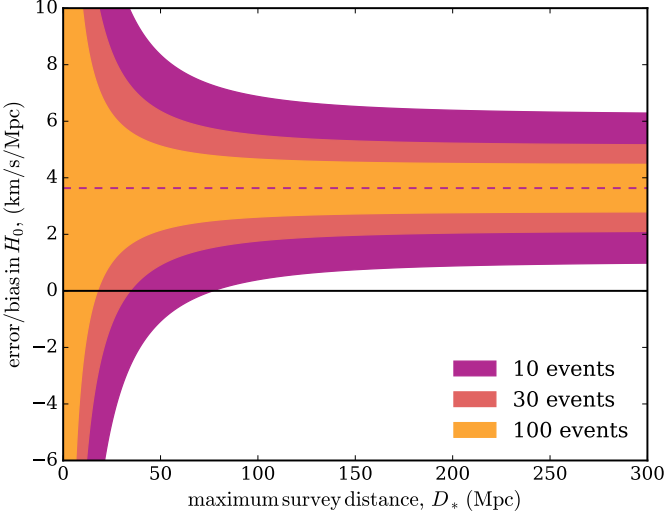


FIG. 1. The expected range of H_0 estimates from sample of $N = 10$, $N = 30$ and $N = 100$ BNS merger events, as a function of the maximum distance, D_* , to which sources can be detected. The offset from zero comes from the potential bias due to selection effects, which would dominate over sample variance for $N \gtrsim 10$ and $D_* \gtrsim 70$ Mpc.

a systematic overestimate of H_0 (e.g., [63, 64]). Mispecification of the cosmological model or the BNS population could also lead to biases.

The main aim of this paper is to test whether a Bayesian population analysis (of the sort described by Refs [46, 53, 54, 58, 63, 65, 66]) gives unbiased H_0 estimates with valid uncertainties (*i.e.*, is both accurate and precise) when applied to realistic BNS merger samples. A secondary aim is to provide a derivation from first principles, applicable in an arbitrary cosmological setting, of the full posterior distribution appropriate to a sample of BNS mergers with counterparts. Simple predictions for the uncertainty and selection bias in H_0 are given in Secs II and III. The sample simulations are described in Sec. IV and the Bayesian analysis approach summarized in Sec. V. The large-sample properties of this approach are then explored in Sec. VI, with the conclusions and possibilities for future development summarized in Sec. VII. The general model and inference formalism is presented in Appendix A and the simplified BNS inspiral model is described in Appendix B.

II. PREDICTED UNCERTAINTIES

In order to assess the performance of any data analysis method it is useful to have a prediction for the expected uncertainties in the idealized case. This gives a target for the uncertainties obtained by analyzing real data and also a guide for assessing whether any potential systematic effects are likely to be significant.

For a local sample of BNS mergers with counterparts,

the predicted uncertainty in H_0 can be estimated by considering Euclidean geometry in which distance is related to redshift by $D = c z / H_0$, where c is the speed of light. Given a measured (spectroscopic) redshift, \hat{z} , an estimated peculiar velocity, \hat{v} and a GW distance, \hat{D} , for a BNS merger event (or any other low-redshift extragalactic object), the natural estimator for the Hubble constant is

$$\hat{H}_0 = \frac{c \hat{z} - \hat{v}}{\hat{D}}, \quad (1)$$

where the peculiar velocity estimate effectively corrects the spectroscopic redshift to (hopefully) bring it closer to the cosmological value. The resultant uncertainty (really the standard deviation of the estimator) is approximated to leading order as (*cf.* [53, 62])

$$\sigma_H \simeq \frac{1}{D} (c^2 \sigma_z^2 + \sigma_v^2 + H_0^2 \sigma_D^2)^{1/2}, \quad (2)$$

where σ_D is the uncertainty in the distance from the GW data, σ_z is the redshift uncertainty, and σ_v is the uncertainty in the peculiar velocity (which should be no larger than the observed peculiar velocity dispersion of ~ 200 km s $^{-1}$ [67], but could be smaller if object-specific information is available).

Using representative numerical values for BNS mergers, and exploiting the fact that it is already known that H_0 is close to 70 km s $^{-1}$ Mpc $^{-1}$, Eq. 2 can be re-written as

$$\sigma_H \simeq 12 \text{ km s}^{-1} \text{ Mpc}^{-1} \left(\frac{D}{100 \text{ Mpc}} \right)^{-1} \times \left[\left(\frac{9.4 \sigma_z}{0.001} \right)^2 + \left(\frac{3.5 \sigma_v}{200 \text{ km s}^{-1}} \right)^2 + \left(\frac{\sigma_D}{10 \text{ Mpc}} \right)^2 \right]^{1/2}. \quad (3)$$

This illustrates that the error in the reconstruction of the source distance from the GW data will be the dominant uncertainty unless the SNR is sufficiently high that σ_D can be reduced to $\lesssim 3$ Mpc, which might be possible for very nearby sources (*e.g.*, the ‘golden’ events invoked in Ref. [53]). Even for such sources, however, there would be little value in obtaining a redshift measurement more precise than the fiducial value of $\sigma_z \simeq 0.001$ unless the peculiar velocity uncertainty of the host could be reduced significantly below the cosmological prior value.

A single BNS merger clearly cannot place interesting constraints on H_0 , but if the uncertainty from a sample of N events scales as $N^{-1/2}$ then Eq. 3 broadly confirms the expectation [53, 54] that ~ 50 events should yield $\sigma_H \lesssim 2$ km s $^{-1}$ Mpc $^{-1}$ and hence be able to resolve the current Hubble constant tension. For the purposes of making quantitative predictions, it is useful to take a more realistic approach that incorporates both the dependence of the uncertainty on source distance and the relative numbers of sources at different distances.

For a given source the GW strain signal is inversely proportional to its distance, while the strain noise is additive and a characteristic of the detector (*e.g.*, [68]).

Assuming the sources are all intrinsically similar (*i.e.*, truly ‘standard’ sirens), the SNR can then be written as $\rho \simeq \rho_* D_*/D$, where ρ_* is the minimum SNR required for selection and D_* is the maximum distance out to which the survey can detect such sources. Assuming further that the relative uncertainty in the distance reconstruction is related to the SNR by $\sigma_D/D \simeq 1/\rho$, the absolute distance uncertainty is (*cf.* [62, 68, 69])

$$\sigma_D \simeq \frac{D^2}{D_*^2} \sigma_*, \quad (4)$$

where σ_* is the distance uncertainty for a source at D_* . Combining this with Eq. 2 gives

$$\sigma_H \simeq H_0 \frac{\sigma_*}{D_*} \left(\frac{D_0^2}{D^2} + \frac{D^2}{D_*^2} \right)^{1/2}, \quad (5)$$

where $D_0 = (c^2 \sigma_z^2 + \sigma_v^2)^{1/2} / (H_0 \sigma_* / D_*) \simeq 30$ Mpc is the distance beyond which redshift/velocity uncertainties become unimportant. This relationship also identifies a distance of $\sim (D_0 D_*)^{1/2} \simeq 30 (D_* / D_0)^{1/2}$ Mpc as that for which a single source in such a survey would yield the tightest constraint on H_0 (*cf.* the ‘sweet spot’ distance of Ref. [53]).

The number of detected sources will, out to $\sim D_*$, be proportional to the volume element, which for the purposes of this calculation can be approximated as $dV/dD \simeq 4\pi D^2$. Ignoring the effect of noise on completeness (which is discussed below in Sec. III and Sec. IV D), the probability of selection, S , is $P(S|D, D_*) = \Theta(D_* - D)$ and so the distance distribution of detected events is then

$$P(D|S, D_*) \simeq \Theta(D) \Theta(D_* - D) \frac{3D^2}{D_*^3}, \quad (6)$$

where $\Theta(\cdot)$ denotes the Heaviside step function.

The optimal estimate from a sample of BNS events would be to take an inverse variance-weighted average of \hat{H}_0 from Eq. 1 for each source, with the weighting proportional to $1/\sigma_H^2$ from Eq. 5. The resultant uncertainty in H_0 for a given sample of N sources would then be $\sigma_H = 1/(\sum_{i=1}^N \sigma_{H,i}^2)$. However, because the number of sources increases as D^2 and the variance in H_0 decreases as D^{-2} , the uncertainty produced by weighting all sources equally is within $\sim 10\%$ of that given by the optimal scheme, so uniform weighting is used here for simplicity. The expected uncertainty from a sample of N events is hence approximated as the average of the expected variance per event,

$$\begin{aligned} \sigma_H &\simeq \left[\frac{1}{N} \int_0^\infty dD P(D|S, D_*) \sigma_D^2 \right]^{1/2} \\ &= \frac{1}{N^{1/2}} \left[\int_0^{D_*} dD \frac{3D^2}{D_*^3} \left(H_0 \frac{\sigma_*}{D_*} \right)^2 \left(\frac{D_0^2}{D^2} + \frac{D^2}{D_*^2} \right) \right]^{1/2} \\ &= \frac{1}{N^{1/2}} \left(\frac{3}{5} \right)^{1/2} \frac{H_0 \sigma_*}{D_*} \left(5 \frac{D_0^2}{D_*^2} + 1 \right)^{1/2}, \end{aligned} \quad (7)$$

where Eqs. 4 and 5 have been used. These uncertainties are shown for different sample sizes as the coloured bands in Fig. 1, from which it is clear that redshift and velocity uncertainties become irrelevant for sufficiently deep surveys with $D_* \gg D_0 \simeq 30$ Mpc. In this regime Eq. 7 simplifies to be

$$\sigma_H \simeq 1.2 \text{ km s}^{-1} \text{ Mpc}^{-1} \left(\frac{N}{50} \right)^{-1/2} \left(\frac{\sigma_*/D_*}{0.15} \right), \quad (8)$$

where the fiducial value chosen for σ_*/D_* is, from simulations, found to be approximately $2/\rho_*$.

Equation 7 (or, if appropriate, Eq. 8) represents a target for any analysis of real or simulated BNS merger data, and also provides a guide to the level at which potential biases could have a significant impact.

III. SELECTION BIAS

Given that it is likely that GW observations of BNS mergers will soon produce uncertainties in H_0 sufficiently small to resolve the current Hubble constant tension, it is important to ensure that the resultant estimates are not significantly affected by systematic biases. There can be systematic errors from model mis-specification, but the most pernicious potential bias comes from the fact that any real BNS merger sample will consist of sources selected on the basis of the measured SNR of the same GW data that is then used to obtain distance constraints. This selection cut will preferentially include cases where the measurement noise has added to the signal, and which hence are inferred to be closer than they in fact are; applying any sort of simple average (*e.g.*, using Eq. 1) to such a BNS merger sample would overestimate H_0 .

The magnitude of this potential bias is somewhat ambiguous, as it is only defined in the context of a specific method for obtaining a distance estimate, \hat{D} , from the GW data, but a reasonable approach is to extend the simple survey model described in Sec. II by including selection effects. The error in H_0 from a single object at distance D for which the data give a distance estimate that is off by $\Delta D = \hat{D} - D$ is

$$\begin{aligned} \hat{H}_0 - H_0 &\simeq -\frac{\Delta D}{D} H_0 \\ &\simeq -10 \text{ km s}^{-1} \text{ Mpc}^{-1} \frac{\Delta D/D}{0.15}, \end{aligned} \quad (9)$$

where the (cosmological) redshift is assumed to be known perfectly and the final expression is reasonable for an object that is close to the detection threshold.

The implied bias from a sample would then be given by averaging $\hat{H}_0 - H_0$ over all distances and possible noise realizations, which would require an explicit model for the measurement process. A more generic approximation is possible by considering the distinct behaviour in three different distance ranges: objects with $D \lesssim D_* - \sigma_*$ are

all well detected, irrespective of the noise realization, and so dilute any overall bias; objects with $|D - D_*| \lesssim \sigma_*$ are detected only if the noise augments the signal, in which case their distance is underestimated by $\Delta D \simeq \sigma_*$; and objects with $D \gtrsim D_* + \sigma_*$ are never detected and so do not affect the Hubble constant estimate at all. Taking the distance distribution of detected objects as

$$P(D|S) \propto \begin{cases} D^2 & \text{if } 0 \leq D \leq D_* - \sigma_* \\ (D_* + \sigma_* - D)(D_* - \sigma)^2 / (2\sigma_*) & \text{if } D_* - \sigma_* \leq D \leq D_* + \sigma_* \\ 0 & \text{if } D > D_* + \sigma_*, \end{cases} \quad (10)$$

the bias from selection effects would be

$$\begin{aligned} \Delta H_{\text{sel}} &\simeq \frac{3}{1 + 2\sigma_*/D_*} \left(\frac{\sigma_*}{D_*} \right)^2 H_0 \\ &\simeq 3.6 \text{ km s}^{-1} \text{ Mpc}^{-1} \left(\frac{\sigma_*/D_*}{0.15} \right)^2. \end{aligned} \quad (11)$$

The $(\sigma_*/D_*)^2$ scaling comes about as this ratio determines both the range of distances for which selection effects are important and the magnitude of the distance underestimate for the fraction of these objects selected. This bias is shown as the offset in Fig. 1 and, aside from being comparable to the current difference between the local and cosmological H_0 measurements (Sec. I), is larger than the predicted uncertainties (Sec. II) from a sample of even $N \simeq 10$ events if $D_* \gtrsim 70$ Mpc. While the exact value of the predicted H_0 bias is somewhat model-dependent, it is clear that it must be taken into account if BNS mergers are to be useful in resolving the current Hubble tension.

IV. SIMULATED BNS MERGER SAMPLES

In order to test both the precision and accuracy of H_0 estimates from BNS mergers it is necessary to generate simulated samples of events that, in particular, are subject to appropriate selection effects. The population model and observations described here represent a specific version of the general structure described in Appendix A. The primary focus is on the self-consistency of the model, with the sample selection being performed on the same measured quantities which are subsequently used to drive the inference calculation. As such, the model is reasonably simple, and includes neither realistic detector and noise models (*cf.* [44, 53, 54]) nor full inference of the individual BNS merger parameters (*cf.* [46, 50, 54]).

A. Cosmology

For the low redshifts of $z \lesssim 0.2$ out to which BNS mergers (and NS-BH mergers) are likely to be detected in the

next decade it is sufficient to adopt the standard Taylor series approximation to the cosmological expansion history, in which the dynamics are characterized to leading order by the deceleration parameter q_0 (*e.g.*, [70]) In a Λ CDM model $q_0 = \Omega_m/2 - \Omega_\Lambda$, where Ω_m is the normalized matter density and Ω_Λ is the normalized cosmological constant. The *Planck* CMB data imply that $\Omega_m \simeq 0.31$ and $\Omega_\Lambda \simeq 0.69$ [2] and hence that $q_0 \simeq -0.53$, although these values would come into question if the *Planck* value of H_0 were determined to be incorrect.

In this cosmological model the luminosity distance is

$$D(z, H_0, q_0) \simeq \frac{c z}{H_0} \left[1 + \frac{1}{2} (1 - q_0) z \right] \quad (12)$$

and the co-moving volume element is

$$\frac{dV}{dz}(H_0, q_0) \simeq 4\pi \frac{c^3 z^2}{H_0^3} [1 - 2(1 + q_0)z]. \quad (13)$$

B. BNS population

The local BNS population is taken to be defined by the rate of mergers per unit proper time per unit co-moving volume, Γ , which has been measured as $\Gamma = 1540^{+3200}_{-1220} \text{ Gpc}^{-3} \text{ yr}^{-1}$ [49].

An individual BNS merger can, as discussed further in Appendix B, effectively be described by just two parameters: its chirp mass, $\mathcal{M} = (M_1 M_2)^{3/5} / (M_1 + M_2)^{1/5}$, where M_1 and M_2 are the masses of the two NSs; and the inclination of the system to the line-of-sight, ι . The population prior distribution in these parameters is taken to have the redshift-independent form

$$P(\mathcal{M}, \iota | \bar{\mathcal{M}}, \sigma_{\mathcal{M}}) \propto N(\mathcal{M}; \bar{\mathcal{M}}, \sigma_{\mathcal{M}}^2) \Theta(\iota) \Theta(\pi - \iota) \frac{\sin(\iota)}{2}, \quad (14)$$

where¹ the sinusoidal distribution in ι encodes the assumption that these systems have random (and independent) orientations.

The distribution of host (line-of-sight) peculiar motions is taken to be

$$P(v | \sigma_{||}) = N(v; 0, \sigma_{||}^2), \quad (15)$$

where $\sigma_{||} \simeq 500 \text{ km s}^{-1}$ from observations of local galaxy motions [67]. The additional motion of the BNS system relative to the host is unimportant in this context (Appendix B).

C. Observations

Three distinct types of measurement provide information about the properties of a BNS merger event with

¹ Here $N(x; \mu, \sigma^2) = \exp[(x - \mu)^2 / (2\sigma^2)] / [(2\pi)^{1/2} \sigma]$ denotes a normal density of mean μ and variance σ^2 .

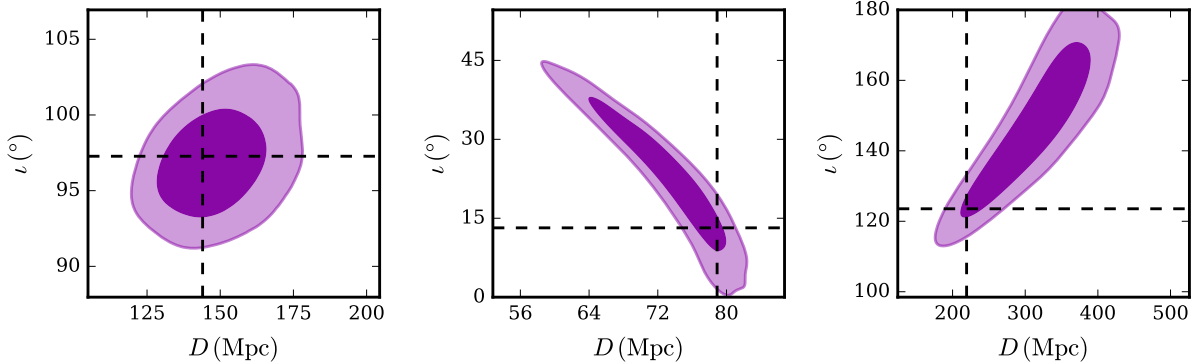


FIG. 2. Constraints on the distance, D , and inclination, ι , for three representative objects from the GW data only. The purple and mauve indicate 68 per cent and 95 per cent highest posterior density credible regions.

a confirmed host: the GW data; the host galaxy redshift measurement; and, potentially, an estimated (line-of-sight) peculiar velocity. Following the general formalism in Appendix A 2, the associated likelihoods depend on the details of the relevant observations and measurements, which are denoted by O for brevity.

The GW data from a single detector comprise the discretized and noisy linear combination of the two GW strains weighted by the detector antenna response function. A full analysis would require a complex parameter estimation pipeline such as **LALInference** [50]. Fortunately, in the inspiral phase the relevant information is well-encoded by three statistics [44]: a very precise measurement of the redshifted chirp mass, $\hat{\mathcal{M}}_z$; and the measured amplitudes of the two orthogonal strain components, \hat{A}_+ and \hat{A}_\times . Assuming the redshifted chirp mass can be measured to infinite precision, and both amplitude measurements have equal uncertainties σ_A , the likelihood effectively takes the form (Appendix B)

$$\begin{aligned} & P(\hat{\mathcal{M}}_z, \hat{A}_+, \hat{A}_\times | \mathcal{M}, \iota, z, H_0, q_0, \sigma_A) \\ &= \delta[\hat{\mathcal{M}}_z - (1+z)\mathcal{M}] \\ &\quad \times N\left[\hat{A}_+; \frac{G(1+z)\mathcal{M}/c^2}{D(z, H_0, q_0)} \frac{1 + \cos^2(\iota)}{2}, \sigma_A^2\right] \\ &\quad \times N\left[\hat{A}_\times; -\frac{G(1+z)\mathcal{M}/c^2}{D(z, H_0, q_0)} \cos(\iota), \sigma_A^2\right], \end{aligned} \quad (16)$$

where² $D(z, H_0, q_0)$ is the luminosity distance as defined in Sec. IV A. The behaviour of this model is illustrated in Fig. 2, which shows three examples of the posterior distributions that would result from analyzing the GW data in isolation for individual mergers. There is a range of morphologies and the strong distance-inclination degeneracy is apparent despite the comparative mathematical simplicity of the model; it is these likelihoods that are

incorporated into the inference formalism described in Sec. V.

The reported spectroscopic redshift of a BNS host, \hat{z} , is taken to have a measurement uncertainty σ_z , with the associated likelihood

$$P(\hat{z}|z, v, \sigma_z) = N\left[\hat{z}; z + (1+z)\frac{v}{c}, \sigma_z^2\right]. \quad (17)$$

Any BNS merger event with a confirmed host galaxy is likely to be of considerable scientific interest, implying that high-quality spectroscopic data will be obtained, so a typical uncertainty would be $\sigma_z \lesssim 0.001$ (cf. the measurement of $\sigma_z = 0.00024$ for the host of GW 170807 [71]).

It is possible that the (line-of-sight) peculiar velocity of a BNS host can be estimated from the positions and/or motions of nearby galaxies, yielding an estimate \hat{v} , with associated uncertainty σ_v . The associated likelihood is hence taken to be

$$P(\hat{v}|v, \sigma_v) = N(\hat{v}; v, \sigma_v^2). \quad (18)$$

The case in which there is no useful peculiar velocity information can be encoded by taking $\sigma_v \rightarrow \infty$, (and, optionally, $\hat{v} = 0$), in which case the uncertainty on the peculiar velocity is given by the value of $\sigma_{||}$ assumed from Sec. IV B.

D. Selection function

The selection of a BNS merger event into the survey is assumed to be determined by the GW data alone, and to take the form of a hard cut on the observed SNR, ρ_* . For the simple model described in Appendix B, with measured strain amplitudes of \hat{A}_+ and \hat{A}_\times and uncertainty σ_A , the observed SNR is

$$\hat{\rho} = \frac{(\hat{A}_+^2 + \hat{A}_\times^2)^{1/2}}{\sigma_A}. \quad (19)$$

² Here $\delta(x)$ denotes a Dirac delta function.

The selection probability is then

$$P(S|\hat{A}_+, \hat{A}_\times, \sigma_A) = \Theta \left[\frac{(\hat{A}_+^2 + \hat{A}_\times^2)^{1/2}}{\sigma_A} - \rho_* \right]. \quad (20)$$

The implied selection function is given in terms of the chirp mass, \mathcal{M} , inclination ι and source distance D as

$$\begin{aligned} P(S|\mathcal{M}, \iota, z, H_0, q_0, \sigma_A, \rho_*) &= \int d\hat{A}_+ \int d\hat{A}_\times P(\hat{A}_+, \hat{A}_\times | \mathcal{M}, \iota, z, H_0, q_0, \sigma_A) P(S|\hat{A}_+, \hat{A}_\times, \sigma_A) \\ &= 1 - \frac{1}{\pi} \int_0^{\phi_{\max}} d\phi \{ \exp[-r_{\min}^2(\phi)/2] - \exp[-r_{\max}^2(\phi)/2] \}, \end{aligned} \quad (21)$$

where $\phi_{\max} = \min[\arcsin(\rho/\rho_*), \pi]$,

$$r_{\min}(\phi) = \max \left\{ 0, \rho \cos(\phi) - [\rho_*^2 - \rho^2 \sin^2(\phi)]^{1/2} \right\}, \quad (22)$$

$$r_{\max}(\phi) = \rho \cos(\phi) + [\rho_*^2 - \rho^2 \sin^2(\phi)]^{1/2},$$

and

$$\rho = \frac{G(1+z)\mathcal{M}/c^2}{D(z, H_0, q_0)} \frac{[\cos^4(\iota) + 6\cos^2(\iota) + 1]^{1/2}}{2} \frac{1}{\sigma_A} \quad (23)$$

is, from Eq. 16, the mean SNR (*cf.* [68]). The combination of additive noise and the inverse distance dependence effectively defines a maximum distance out to which a survey can detect sources. For the simple model defined by Eq. 16, and assuming redshifts of $z \ll 1$, this is given by $D_* \simeq G\mathcal{M}/c^2/(\rho_* \sigma_A)$, but in many cases (*e.g.*, Sec. II) it is most useful to think of D_* as a characteristic of a survey.

In reality, the selection of a sample of BNS merger events with confirmed hosts also depends on whether it is possible to confirm a host galaxy from EM follow-up observations (*e.g.*, [58]). For the moment all GW events are going to be the subject of intense follow-up observing campaigns, and so it is assumed here both that every BNS event that occurs in a galaxy will have its host identified and, further, that a spectroscopic redshift measurement will subsequently be made. While some fraction of events might be host-less (*e.g.* [72, 73]) this will just reduce the useful sample size produced by any given survey; the inference of H_0 should not be affected.

E. Expected number of events

Assuming BNS mergers are independent of each other, and the parent population of BNS systems is large, it is reasonable to model the sample size, N , as a draw from a Poisson distribution. This is characterized purely by the expected number of events, which (as described further in Appendix A 3b) is given by integrating over the BNS

parameters and the observing period T to obtain

$$\begin{aligned} \bar{N}(\Gamma, \bar{\mathcal{M}}, \sigma_{\mathcal{M}}, H_0, q_0, \sigma_A, \rho_*, T) &= T \int_0^\infty dz \frac{\Gamma}{1+z} \frac{dV}{dz}(H_0, q_0) \\ &\quad \int_0^\infty d\mathcal{M} \int_0^\pi d\iota P(\mathcal{M}, \iota | \bar{\mathcal{M}}, \sigma_{\mathcal{M}}) P(S|\mathcal{M}, \iota, z, H_0, q_0, \sigma_A, \rho_*), \end{aligned} \quad (24)$$

where $P(\mathcal{M}, \iota | \bar{\mathcal{M}}, \sigma_{\mathcal{M}})$ is given in Eq. 14 and $P(S|\mathcal{M}, \iota, z, H_0, q_0, \sigma_A, \rho_*)$ is given in Eq. 21. In general, these integrals must be evaluated numerically, *e.g.*, using a Monte Carlo approach such as that described below in Sec. IV F.

Particular care needs to be taken here as the Gaussian GW noise model defined in Sec. IV C results in a non-zero selection probability even for sources at an infinite distance with a true SNR of $\rho = 0$. Given that the volume element as specified in Sec. IV B potentially increases to infinite redshifts, the combination is an unnormalizable distribution with an infinite number of expected sources. This is not a problem in practice as the integration in Eq. 24 can be truncated at any finite redshift beyond the detection horizon; this model is hence best understood as a numerical approximation.

Another important aspect of Eq. 24 is that \bar{N} is nearly independent of H_0 , and can hence potentially be ignored in the data analysis step. For low redshifts the comoving volume element scales as H_0^{-3} , but the effective maximum redshift of the survey is $z_* \simeq H_0 D_*/c \propto H_0$, so the implied volume in redshift space scales as H_0^3 ; the two effects cancel out to leading order (*cf.* [46, 53]). This result can also be understood from a purely physical point of view: the detectability of a GW event is not significantly affected by its recession velocity; only its (luminosity) distance is important, and so changing the radial integration variable to D would (largely) remove H_0 from the calculation.

F. Simulation algorithm

The algorithm used here to generate a self-consistently selected sample of low-redshift BNS merger events (as used in Sec. VI) is:

1. Choose values of the cosmological model parameters, H_0 and q_0 (Sec. IV A), and BNS population properties, Γ , $\bar{\mathcal{M}}$ and $\sigma_{\mathcal{M}}$ (Sec. IV B), along with the observational characteristics of the GW and EM observations, T , σ_A , ρ_* , σ_z and σ_v (Sec. IV C).
2. Identify a maximum redshift

$$z_{\max} \simeq \frac{G H_0}{c^3} \frac{\bar{\mathcal{M}} + 3\sigma_{\mathcal{M}}}{(\rho_* - 3)\sigma_A}, \quad (25)$$

beyond which the probability of a GW detection for even the most massive BNS merger is negligible (but stopping short of the spurious second peak discussed in Sec. IV E).

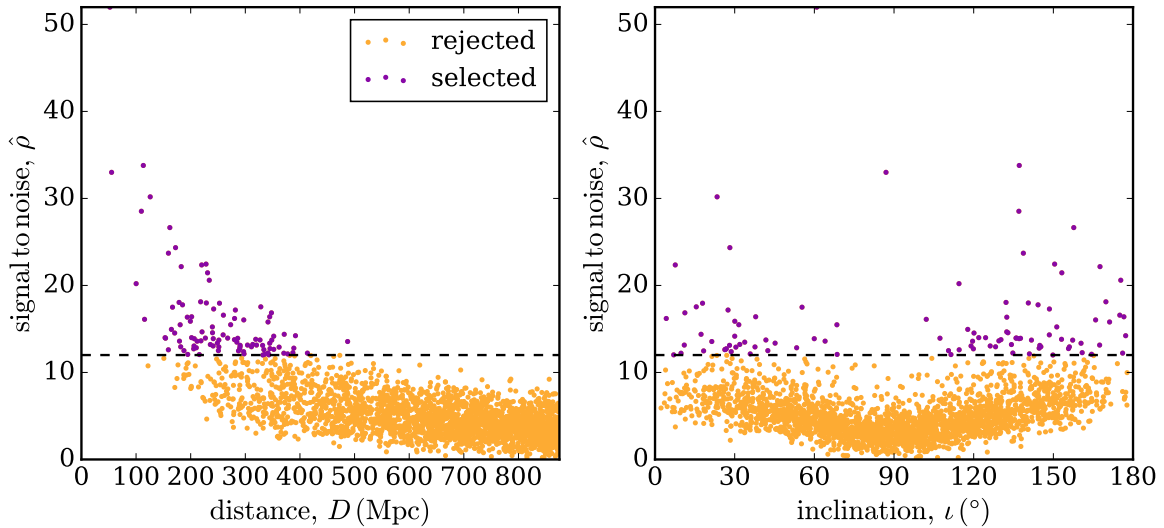


FIG. 3. Distributions of the measured SNR, $\hat{\rho}$, and distance (left) and inclination (right) for a simulated sample of 100 selected BNS merger events (purple) with $\rho \geq \rho_* = 12$. The much larger number of mergers which were not selected are also shown in orange.

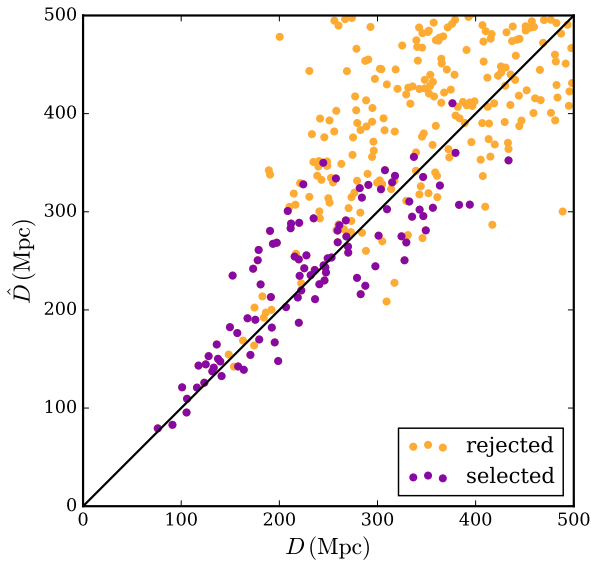


FIG. 4. Comparison of the fiducial best-fit distance, \hat{D} , to the true distance, D , for both selected (purple) and rejected (orange) sources. The over-abundance of sources close to the maximum survey distance with $\hat{D} < D$ would potentially give a biased estimate of H_0 , as described in Sec. III.

3. Calculate the expected number of mergers with $z \leq z_{\max}$ during the observing period T as

$$\bar{N}_{\max} = T \int_0^{z_{\max}} dz \frac{\Gamma}{1+z} \frac{dV}{dz}(H_0, q_0). \quad (26)$$

Draw the actual number of mergers in this volume, N_{\max} , from a Poisson distribution of mean \bar{N}_{\max} .

4. For each of these N_{\max} BNS mergers:

(a) Draw a redshift from the distribution

$$\begin{aligned} & P(z|z_{\max}, H_0, q_0) \\ & \propto \Theta(z) \Theta(z_{\max} - z) \frac{1}{1+z} \frac{dV}{dz}(H_0, q_0), \quad (27) \end{aligned}$$

and both a chirp mass and inclination from $P(\mathcal{M}, \iota | \bar{\mathcal{M}}, \sigma_{\mathcal{M}})$ as given in Eq. 14.

- (b) Draw measured amplitudes \hat{A}_+ and \hat{A}_\times (and, optionally, a measured chirp mass, \hat{M}_z) from Eq. 16, and hence calculate the observed SNR, $\hat{\rho} = \rho(\hat{A}_+, \hat{A}_\times, \sigma_A)$, according to Eq. 19.
- (c) Select the merger into the sample of detected events if $\hat{\rho} \geq \rho_*$.
- (d) If the merger is selected then draw a host peculiar velocity v from Eq. 15, a measured redshift from Eq. 17 and, optionally, a measured peculiar velocity from Eq. 18.

The output of the above algorithm is a sample of N detected BNS mergers along with their redshifted chirp masses, $\hat{\mathcal{M}}_z = (\hat{\mathcal{M}}_{z,1}, \hat{\mathcal{M}}_{z,2}, \dots, \hat{\mathcal{M}}_{z,N})$, measured GW amplitudes, $\hat{\mathbf{A}} = (\hat{A}_{+,1}, \hat{A}_{\times,1}, \hat{A}_{+,2}, \hat{A}_{\times,2}, \dots, \hat{A}_{+,N}, \hat{A}_{\times,N})$, their hosts' spectroscopic redshifts, $\hat{z} = (\hat{z}_1, \hat{z}_2, \dots, \hat{z}_N)$, and (possibly) their estimated peculiar velocities, $\hat{\mathbf{v}} = (\hat{v}_1, \hat{v}_2, \dots, \hat{v}_N)$, along with the associated measurement uncertainties. The algorithm also produces the true redshifts, $z = (z_1, z_2, \dots, z_N)$, chirp masses, $\mathcal{M} = (\mathcal{M}_1, \mathcal{M}_2, \dots, \mathcal{M}_N)$, inclinations, $\iota = (\iota_1, \iota_2, \dots, \iota_N)$, and host peculiar velocities, $\mathbf{v} = (v_1, v_2, \dots, v_N)$, for these selected mergers, although these quantities are not actually part of a simulated

catalog, and cannot be used in the parameter inference described in Sec. V.

One important feature of the above approach is that, while N is a draw from the appropriate Poisson distribution of mean \bar{N} , the integral in Eq. 24 is never actually evaluated. This is not particularly important for the fairly simple model used here, but is potentially critical in the more general cosmological case described in Appendix A 1. An example of a sample generated in this way is shown in Fig. 3, in particular illustrating that the most distant detected sources in the sample are those for which the noise has conspired to increase the SNR. These are also typically face-on or face-off sources, despite these configurations having a low prior probability (Eq. 14). If such data were treated naively, it would produce systematic underestimates for the distances to mergers close to the maximum survey distance. For the sample shown in Fig. 4 this would induce a bias of $\sim 2 \text{ km s}^{-1} \text{ Mpc}^{-1}$ in the inferred value of H_0 (cf. Sec. III).

V. BAYESIAN PARAMETER INFERENCE

A sample of BNS mergers with measured GW data, spectroscopic host redshifts and (possibly) estimated peculiar velocities places constraints on the cosmological model, the BNS population and the properties of the mergers. This is encoded in the joint posterior distribution of all the parameters. For the population and data model described above in Sec. IV this has the form $P(\mathcal{M}, \iota, z, v, \Gamma, \bar{\mathcal{M}}, \sigma_{\mathcal{M}}, H_0, q_0 | N, \hat{\mathcal{M}}_z, \hat{A}, \hat{z}, \hat{v}, \sigma_A, \sigma_z, \sigma_v, \rho_*, T, I)$, where I represents the prior information assumed about the cosmological and BNS population parameters. A derivation from first principles of the general form of this posterior distribution, valid for arbitrary cosmologies and BNS population models, is given in Sec. A 4. This has the same structure and dependencies as the simpler model described in Sec. IV, so the above posterior can be obtained from Eq. A9 by making the identifications $\theta \rightarrow \mathcal{M}$, $\beta \rightarrow (\Gamma, \bar{\mathcal{M}}, \sigma_{\mathcal{M}})$, $\Omega \rightarrow (H_0, q_0)$ and $O \rightarrow (\sigma_A, \sigma_z, \sigma_v, \rho_*, T)$. This gives

$$\begin{aligned} & P(\mathcal{M}, \iota, z, v, \Gamma, \bar{\mathcal{M}}, \sigma_{\mathcal{M}}, H_0, q_0 | N, \hat{\mathcal{M}}_z, \hat{A}, \hat{z}, \hat{v}, \sigma_A, \sigma_z, \sigma_v, \rho_*, T, I) \\ & \propto P(\Gamma, \bar{\mathcal{M}}, \sigma_{\mathcal{M}} | I) P(H_0, q_0 | I) \exp[-\bar{N}(\Gamma, \bar{\mathcal{M}}, \sigma_{\mathcal{M}}, H_0, q_0, \sigma_A, \rho_*, T)] \\ & \times \prod_{i=1}^N \frac{\Gamma}{1+z_i} \frac{dV}{dz}(H_0, q_0) P(\mathcal{M}_i, \iota_i; \bar{\mathcal{M}}, \sigma_{\mathcal{M}}) P(\hat{\mathcal{M}}_{z,i}, \hat{A}_{+,i}, \hat{A}_{\times,i} | \mathcal{M}_i, \iota_i, z_i, H_0, q_0, \sigma_A) P(v_i | \sigma_{||}) P(\hat{z}_i | z_i, v_i, \sigma_z) P(\hat{v}_i | v_i, \sigma_v), \end{aligned} \quad (28)$$

where the expected number of detected mergers $\bar{N}(\Gamma, \bar{\mathcal{M}}, \sigma_{\mathcal{M}}, H_0, q_0, \sigma_A, \rho_*, T)$ is defined in Eq. 24, the volume element $dV/dz(H_0, q_0)$ is given in Eq. 13, the BNS demographic $P(\mathcal{M}, \iota; \bar{\mathcal{M}}, \sigma_{\mathcal{M}})$ is given in Eq. 14, the GW likelihood $P(\hat{\mathcal{M}}_z, \hat{A}_+, \hat{A}_\times | \mathcal{M}, \iota, z, H_0, q_0, \sigma_A)$ is given in Eq. 16, the peculiar velocity prior $P(v | \sigma_{||})$ is given in Eq. 15, the redshift likelihood $P(\hat{z} | z, v, \sigma_z)$ is given in Eq. 17, and the peculiar velocity likelihood $P(\hat{v} | v, \sigma_v)$ is given in Eq. 18.

The prior in the cosmological parameters is taken to be

$$\begin{aligned} & P(H_0, q_0 | I) \\ & \propto N(H_0; \hat{H}_0, \sigma_H^2) \Theta(q_0 + 2) \Theta(1 - q_0) N(q_0; -0.5, 0.5^2), \end{aligned} \quad (29)$$

where the H_0 prior is centred on $\hat{H}_0 = 70 \text{ km s}^{-1} \text{ Mpc}^{-1}$ and has a width of $\sigma_H = 20 \text{ km s}^{-1} \text{ Mpc}^{-1}$. The truncation in q_0 avoids the region of parameter space ($q_0 > 1/2 z_{\max} - 1 \simeq 1.1$) in which dV/dz drops to zero inside the simulation volume described in Sec. IV F. For samples of more than a few BNS mergers these priors have a minimal effect on the inference of H_0 .

The BNS population parameters $\bar{\mathcal{M}}$, $\sigma_{\mathcal{M}}$ and Γ could be fit along with the cosmological parameters, but doing so is prohibitive numerically (as explained below), given the large number of simulations needed for the tests de-

scribed in Sec. VI. The prior in the population parameters is hence taken to be

$$P(\Gamma, \bar{\mathcal{M}}, \sigma_{\mathcal{M}}) = \delta(\Gamma - \hat{\Gamma}) \delta(\bar{\mathcal{M}} - \hat{\mathcal{M}}) \delta(\sigma_{\mathcal{M}} - \hat{\sigma}_{\mathcal{M}}), \quad (30)$$

where the assumed values are $\hat{\Gamma}_0 = 1540 \text{ Gpc}^{-3} \text{ yr}^{-1}$, $\hat{\mathcal{M}} = 1.2 M_\odot$ and $\hat{\sigma}_{\mathcal{M}} = 0.12 M_\odot$.

Evaluating the posterior (Eq. 28) requires calculating the expected number of detectable events, \bar{N} , for different values of the unspecified model parameters: in this case, H_0 and, if relevant, q_0 . Rather than evaluate Eq. 24 at every location in parameter space, it is more efficient to estimate this integral using a Monte Carlo approach for a grid of models and then fit a smooth function to capture its parameter dependence. A 25-point grid of H_0 (and q_0) values and a fourth-order polynomial were used, although the results are insensitive to these specific choices. With this fit in hand, the 402-parameter³ joint posterior for a given catalog was explored using Hamiltonian Monte Carlo [74] as implemented in Stan [75, 76]. This yields ~ 700 independent samples from each marginal H_0 posterior (from 2000 total samples) in 25 seconds on four

³ The parameters are H_0 , q_0 and a true redshift, peculiar velocity, chirp mass and inclination for each of the 100 BNS mergers.

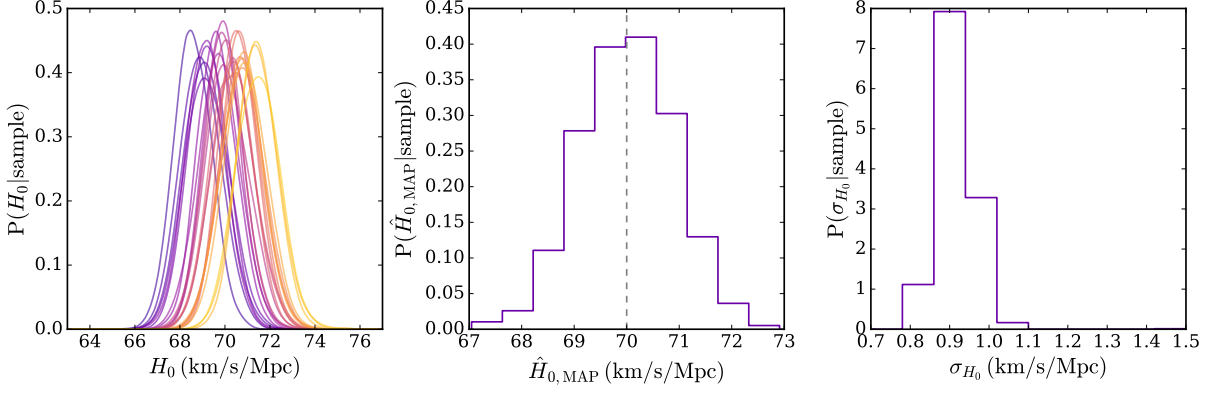


FIG. 5. Left: H_0 posteriors for 25 independent 100-BNS samples, generated assuming a linear Hubble relation. The posteriors are colored dark purple to light orange by their MAP H_0 values. Center/right: distribution of MAP H_0 values and posterior standard deviations for the full set of 1000 100-BNS samples.

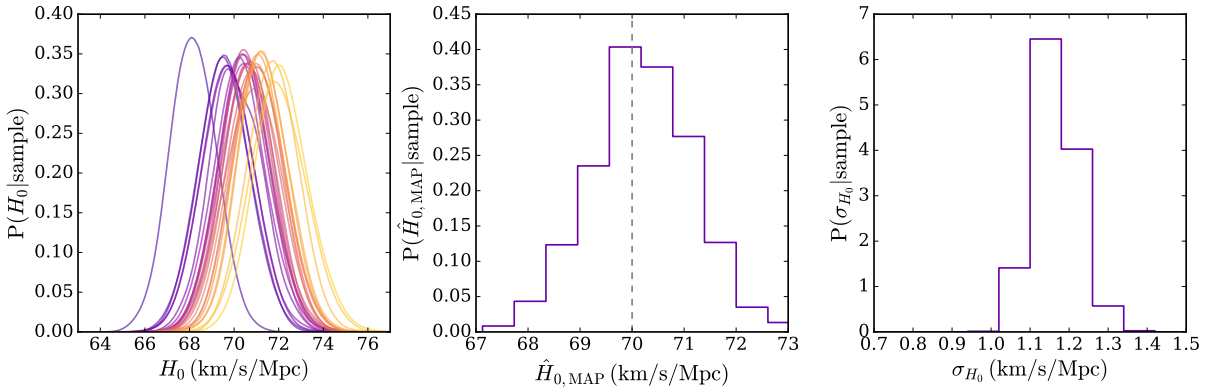


FIG. 6. As Fig. 5, but generated assuming a quadratic Hubble relation. From left to right: example H_0 posteriors, colored from low to high MAP value; distributions of MAP H_0 values and posterior standard deviations for 1000 100-BNS samples.

order	posterior bias	posterior width
linear	0.01 ± 0.89	0.92 ± 0.30
quadratic	0.20 ± 0.97	1.17 ± 0.36

TABLE I. Average bias and width of H_0 posteriors calculated from our 1000 simulations of 100-event samples.

Intel Xeon (2.4 GHz) CPUs, sufficient to analyze large numbers of simulations.

VI. RESULTS

The inference formalism described in Sec. V can be tested on simulated BNS merger samples generated self-consistently as described in Sec. IV F. The datasets were generated with these parameter values: $H_0 = 70 \text{ km s}^{-1} \text{ Mpc}^{-1}$; $q_0 = -0.5$ or a linear Hubble relationship; $\Gamma = 1500 \text{ Gpc}^{-3} \text{ yr}^{-1}$; $\bar{M} = 1.2 M_\odot$; and $\sigma_M = 0.12 M_\odot$. The observations are defined by: $\sigma_A =$

2×10^{-23} ; $\rho_* = 12$; $\sigma_{||} = 500 \text{ km s}^{-1}$; $\sigma_v = 200 \text{ km s}^{-1}$; and $\sigma_z = 0.001$. This set-up gives a maximum survey distance of $D_* \simeq 250 \text{ Mpc}$ and typical Hubble-flow velocity uncertainties of $\sim 360 \text{ km s}^{-1}$.

1000 independent merger catalogs of $N = 100$ selected events were generated for each of two cosmological scenarios: a linear Hubble relationship described by H_0 alone; and the quadratic relationship described by H_0 and q_0 , as set out in Sec. IV A. The resultant posterior distributions in H_0 are shown for 25 independent simulated samples of $N = 100$ mergers in the left panels of Fig. 5 (for the linear Hubble relation) and Fig. 6 (for the quadratic Hubble relation). Samples of this size are clearly approaching the asymptotic Gaussian limit, with the quadratic Hubble relation posteriors slightly broader (and more skewed) than in the linear setting due to the degeneracy between H_0 and q_0 . The right panels of Figs 5 and 6 show the distributions of posterior widths for the full sets of 1000 catalogs. These distributions, whose characteristics are summarized in Table I, show that posteriors formed from samples of 100 BNS mergers have similar uncertainties (with $\sim 33\%$ variations in width),

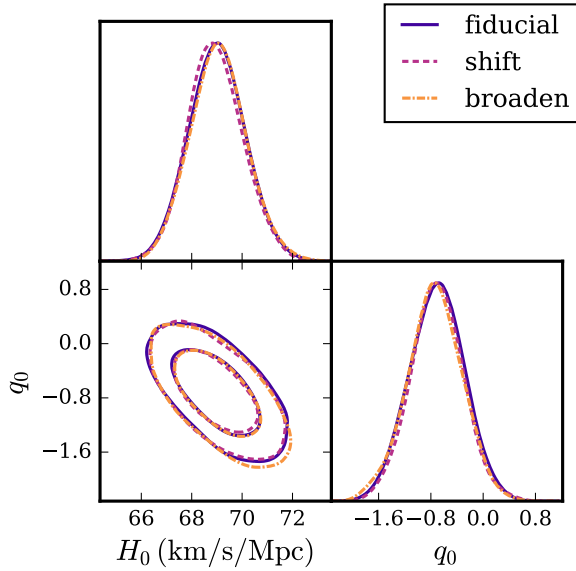


FIG. 7. Constraints on H_0 and q_0 for a single 100-event sample, inferred using our fiducial \mathcal{M} prior (purple solid); a prior shifted upwards by one sigma (pink dashed); and a prior with four times the variance (orange dot-dashed). The inference is robust to reasonable variations in the chirp mass prior.

indicating that there is minimal inter-sample variance. However, the peaks of the H_0 posterior from individual samples can be scattered significantly high or low (as was the case for the single sample used in Ref. [54]).

The distribution of maximum-posterior ($\hat{H}_{0,\text{MAP}}$) values from samples of $N = 100$ events are shown in the center panels of Figs 5 and 6. For both Hubble relations, the distribution of $\hat{H}_{0,\text{MAP}}$ values is centered on the true underlying value, indicating that the method is unbiased in the presence of selection effects. The average bias for the two Hubble relations, defined as the difference between $\hat{H}_{0,\text{MAP}}$ and H_0 , is listed in Table I and is within a standard deviation of zero in both cases.

The robustness of this approach, and particularly the sensitivity of the H_0 constraints to mis-specification of $\bar{\mathcal{M}}$ and $\sigma_{\mathcal{M}}$, can be assessed by conditioning the inference on values for these parameters that are different from those used in the simulations. Figure 7 shows posteriors on H_0 and q_0 inferred using three different BNS population priors for a single 100-event sample with chirp masses generated from the fiducial model (Eq. 14). The joint posteriors obtained for a prior with $\hat{\mathcal{M}} = \bar{\mathcal{M}} + \sigma_{\mathcal{M}}$ and $\hat{\sigma}_{\mathcal{M}} = \sigma_{\mathcal{M}}$ are shown by the pink dashed curves; results for a prior with $\hat{\mathcal{M}} = \bar{\mathcal{M}}$ and $\hat{\sigma}_{\mathcal{M}} = 4\sigma_{\mathcal{M}}$ are shown by the orange dot-dashed curves. The constraints on the cosmological parameters in both cases differ insignificantly from those obtained using the correct model ($\hat{\mathcal{M}} = \bar{\mathcal{M}}$ and $\hat{\sigma}_{\mathcal{M}} = \sigma_{\mathcal{M}}$), as shown by the solid purple curves.

VII. CONCLUSIONS

Using a rigorous Bayesian procedure to analyze realistic samples of BNS mergers gives estimates of the Hubble constant that are unbiased in the presence of selection effects, and robust to mis-specification of the other cosmological parameters or the BNS population model. The resultant uncertainties match expectations, confirming that this method is both accurate and precise. Applying such methods to the sample of ~ 50 BNS mergers that could be produced by LIGO+Virgo in the next ~ 5 years should yield a robust H_0 estimate accurate to less than $2 \text{ km s}^{-1} \text{ Mpc}^{-1}$. This would be sufficient to resolve the current tension between local and cosmological measurements of H_0 .

While the formalism derived and implemented here is very general and applicable in an arbitrary cosmological setting, the primary focus of the simulations was on self-consistency, in particular with the same selection rule(s) used both in the sample generation and the posterior calculations. In order to take such an approach for sufficiently large numbers of simulations, it was necessary to adopt a simplified model of the GW waveform and fix some population-level parameters. One obvious extension of this work would be to use full numerical simulations of BNS and NS-BH inspirals and their resultant time series, using a simplified GW waveform and likelihood analysis such as BAYESTAR [77] or, more ambitiously, LALInference [50]. A single simulated sample of 51 BNS mergers was analyzed using LALInference in Ref. [54], suggesting that even with realistic individual object constraints the regime of asymptotic normality has been reached, but this remains to be demonstrated fully.

While the near-complete decoupling of the BNS mass distribution from the cosmological parameters due to the tight chirp mass constraints is central to this entire method of measuring the Hubble constant [42], it would also be preferable to extend the Bayesian inference formalism to include the population parameters as well, something which will be more important for BNS and NS-BH merger samples for which there are fewer constraints. A related extension would be to include a more realistic model of the EM counterpart detection process, in particular the correlation between GW selection and counterpart identification due to viewing angle dependencies. This will become particularly important in the context of GW-based constraints on H_0 and other cosmological parameters from potential combined samples of hundreds to thousands of BNS, NS-BH and BBH mergers expected in the next decade with upgraded and new GW detectors (e.g., [78, 79]).

VIII. ACKNOWLEDGMENTS

The authors acknowledge useful discussions with Jon Gair and Archisman Ghosh. This work was performed in

part at the Aspen Center for Physics, which is supported by National Science Foundation grant PHY-1607611. The Flatiron Institute is supported by the Simons Foundation. This work was also partially supported by a grant from the Simons Foundation. HVP was partially supported by the European Research Council (ERC) under the European Community's Seventh Framework Programme (FP7/2007-2013)/ERC grant agreement number 306478-CosmicDawn, and the research environment

grant "Gravitational Radiation and Electromagnetic Astrophysical Transients (GREAT)" funded by the Swedish Research Council (VR) under Dnr 2016-06012. This work was partially enabled by funding from the UCL Cosmoparticle Initiative. ARW and SMN acknowledge the generous financial support of the Netherlands Organization for Scientific Research through the NWO VIDI and NWO TOP Grants (PI: Nissanke).

[1] A. G. Riess, S. Casertano, W. Yuan, L. Macri, B. Bucciarelli, M. G. Lattanzi, J. W. MacKenty, J. B. Bowers, W. Zheng, A. V. Filippenko, C. Huang, and R. I. Anderson, *ApJ* **861**, 126 (2018).

[2] Planck Collaboration, ArXiv e-prints (2018), arXiv:1807.06209.

[3] M. Wyman, D. H. Rudd, R. A. Vanderveld, and W. Hu, *PRL* **112**, 051302 (2014).

[4] A. Pourtsidou and T. Tram, *PRD* **94**, 043518 (2016).

[5] E. Di Valentino, A. Melchiorri, and J. Silk, *Physics Letters B* **761**, 242 (2016).

[6] Q.-G. Huang and K. Wang, *EPJC* **76**, 506 (2016).

[7] J. L. Bernal, L. Verde, and A. G. Riess, *JCAP* **10**, 019 (2016).

[8] P. Ko and Y. Tang, *Physics Letters B* **762**, 462 (2016).

[9] T. Karwal and M. Kamionkowski, *PRD* **94**, 103523 (2016).

[10] S. Kumar and R. C. Nunes, *PRD* **94**, 123511 (2016).

[11] B. Santos, A. A. Coley, N. Chandrachani Devi, and J. S. Alcaniz, *JCAP* **2**, 047 (2017).

[12] V. Prilepsina and Y. Tsai, *JHEP* **9**, 33 (2017).

[13] G.-B. Zhao *et al.*, *Nature Astronomy* **1**, 627 (2017).

[14] M.-M. Zhao, D.-Z. He, J.-F. Zhang, and X. Zhang, *PRD* **96**, 043520 (2017).

[15] J. Solà, A. Gómez-Valent, and J. de Cruz Pérez, *Physics Letters B* **774**, 317 (2017).

[16] E. Di Valentino, E. V. Linder, and A. Melchiorri, *PRD* **97**, 043528 (2018).

[17] E. Di Valentino, C. Boehm, E. Hivon, and F. R. Bouchet, *PRD* **97**, 043513 (2018).

[18] L. L. Graef, M. Benetti, and J. S. Alcaniz, ArXiv e-prints (2018), arXiv:1809.04501.

[19] W. Yang, A. Mukherjee, E. Di Valentino, and S. Pan, ArXiv e-prints (2018), arXiv:1809.06883.

[20] A. El-Zant, W. El Hanafy, and S. Elgammal, ArXiv e-prints (2018), arXiv:1809.09390.

[21] G. Benevento, M. Raveri, A. Lazanu, N. Bartolo, M. Liguori, P. Brax, and P. Valageas, ArXiv e-prints (2018), arXiv:1809.09958.

[22] W. Yang, S. Pan, E. Di Valentino, E. N. Sardakis, and S. Chakraborty, ArXiv e-prints (2018), arXiv:1810.05141.

[23] K. Aylor, M. Joy, L. Knox, M. Millea, S. Raghunathan, and W. L. Kimmy Wu, ArXiv e-prints (2018), arXiv:1811.00537.

[24] C.-T. Chiang and A. Slosar, ArXiv e-prints (2018), arXiv:1811.03624.

[25] V. Poulin, T. L. Smith, T. Karwal, and M. Kamionkowski, ArXiv e-prints (2018), arXiv:1811.04083.

[26] G. Efstathiou, *MNRAS* **440**, 1138 (2014).

[27] D. N. Spergel, R. Flauger, and R. Hložek, *PRD* **91**, 023518 (2015).

[28] M. Rigault *et al.*, *ApJ* **802**, 20 (2015).

[29] D. O. Jones, A. G. Riess, and D. M. Scolnic, *ApJ* **812**, 31 (2015).

[30] G. E. Addison, Y. Huang, D. J. Watts, C. L. Bennett, M. Halpern, G. Hinshaw, and J. L. Weiland, *ApJ* **818**, 132 (2016).

[31] Planck Collaboration, *A&A* **596**, A107 (2016).

[32] W. Cardona, M. Kunz, and V. Pettorino, *JCAP* **3**, 056 (2017).

[33] B. R. Zhang, M. J. Childress, T. M. Davis, N. V. Karpenka, C. Lidman, B. P. Schmidt, and M. Smith, *MNRAS* **471**, 2254 (2017).

[34] H.-Y. Wu and D. Huterer, *MNRAS* **471**, 4946 (2017).

[35] S. M. Feeney, D. J. Mortlock, and N. Dalmasso, *MNRAS* **476**, 3861 (2018).

[36] B. Follin and L. Knox, *MNRAS* **477**, 4534 (2018).

[37] S. Dhawan, S. W. Jha, and B. Leibundgut, *A&A* **609**, A72 (2018).

[38] M. Rigault *et al.*, ArXiv e-prints (2018), arXiv:1806.03849.

[39] C. A. P. Bengaly, U. Andrade, and J. S. Alcaniz, ArXiv e-prints (2018), arXiv:1810.04966.

[40] B. P. Abbott, R. Abbott, T. D. Abbott, F. Acernese, K. Ackley, C. Adams, T. Adams, P. Addesso, R. X. Adhikari, V. B. Adya, and et al., *ApJL* **848**, L12 (2017).

[41] B. P. Abbott, R. Abbott, T. D. Abbott, F. Acernese, K. Ackley, C. Adams, T. Adams, P. Addesso, R. X. Adhikari, V. B. Adya, and et al., *ApJL* **848**, L13 (2017).

[42] B. F. Schutz, *Nature* **323**, 310 (1986).

[43] N. Dalal, D. E. Holz, S. A. Hughes, and B. Jain, *PRD* **74**, 063006 (2006).

[44] S. Nissanke, D. E. Holz, S. A. Hughes, N. Dalal, and J. L. Sievers, *ApJ* **725**, 496 (2010).

[45] S. R. Taylor and J. R. Gair, *PRD* **86**, 023502 (2012).

[46] B. P. Abbott *et al.*, *Nature* **551**, 85 (2017).

[47] S. Nissanke, D. E. Holz, N. Dalal, S. A. Hughes, J. L. Sievers, and C. M. Hirata, ArXiv e-prints (2013), arXiv:1307.2638.

[48] S. Vitale and H.-Y. Chen, *PRL* **121**, 021303 (2018).

[49] B. P. Abbott, R. Abbott, T. D. Abbott, F. Acernese, K. Ackley, C. Adams, T. Adams, P. Addesso, R. X. Adhikari, V. B. Adya, and et al., *PRL* **119**, 161101 (2017).

[50] J. Veitch *et al.*, *Phys. Rev.* **D91**, 042003 (2015).

[51] The LIGO Scientific Collaboration and the Virgo Collaboration, ArXiv e-prints (2018), arXiv:1805.11579.

[52] C. Guidorzi, R. Margutti, D. Brout, D. Scolnic, W. Fong, K. D. Alexander, P. S. Cowperthwaite, J. Annis,

E. Berger, P. K. Blanchard, R. Chornock, D. L. Copejans, T. Eftekhari, J. A. Frieman, D. Huterer, M. Nicholl, M. Soares-Santos, G. Terreran, V. A. Villar, and P. K. G. Williams, *ApJL* **851**, L36 (2017).

[53] H.-Y. Chen, M. Fishbach, and D. Holz, *Nature* **562**, 545 (2018).

[54] S. M. Feeney, H. V. Peiris, A. R. Williamson, S. M. Nisanke, D. J. Mortlock, J. Alsing, and D. Scolnic, ArXiv e-prints (2018), arXiv:1802.03404.

[55] W. Del Pozzo, *PRD* **86**, 043011 (2012).

[56] C. Messenger and J. Read, *PRL* **108**, 091101 (2012).

[57] M. Oguri, *PRD* **93**, 083511 (2016).

[58] M. Fishbach, R. Gray, I. Magaña Hernandez, H. Qi, A. Sur, members of the LIGO Scientific Collaboration, and the Virgo Collaboration, ArXiv e-prints (2018), arXiv:1807.05667.

[59] R. Nair, S. Bose, and T. D. Saini, *PRD* **98**, 023502 (2018).

[60] K. Hotokezaka, E. Nakar, O. Gottlieb, S. Nisanke, K. Masuda, G. Hallinan, K. P. Mooley, and A. T. Deller, ArXiv e-prints (2018), arXiv:1806.10596.

[61] K. P. Mooley, A. T. Deller, O. Gottlieb, E. Nakar, G. Hallinan, S. Bourke, D. A. Frail, A. Horesh, A. Corsi, and K. Hotokezaka, *Nature* **561**, 355 (2018).

[62] N. Seto and K. Kyutoku, *MNRAS* **475**, 4133 (2018).

[63] S. R. Taylor, J. R. Gair, and I. Mandel, *PRD* **85**, 023535 (2012).

[64] C. Messenger and J. Veitch, *New Journal of Physics* **15**, 053027 (2013).

[65] B. P. Abbott, R. Abbott, T. D. Abbott, M. R. Abernathy, F. Acernese, K. Ackley, C. Adams, T. Adams, P. Addesso, R. X. Adhikari, and et al., *Physical Review X* **6**, 041015 (2016).

[66] I. Mandel, W. M. Farr, and J. R. Gair, ArXiv e-prints (2018), arXiv:1809.02063.

[67] D. Burstein, *Reports on Progress in Physics* **53**, 421 (1990).

[68] C. Cutler and É. E. Flanagan, *PRD* **49**, 2658 (1994).

[69] D. Marković, *PRD* **48**, 4738 (1993).

[70] S. Weinberg, *Cosmology* (Oxford University Press, 2008).

[71] A. C. Crook, J. P. Huchra, N. Martimbeau, K. L. Masters, T. Jarrett, and L. M. Macri, *ApJ* **655**, 790 (2007).

[72] E. Berger, *ApJ* **722**, 1946 (2010).

[73] W. Fong and E. Berger, *ApJ* **776**, 18 (2013).

[74] R. M. Neal, ArXiv e-prints (2012), arXiv:1206.1901 [stat.CO].

[75] B. Carpenter, A. Gelman, M. Hoffman, D. Lee, B. Goodrich, M. Betancourt, M. Brubaker, J. Guo, P. Li, and A. Riddell, *Journal of Statistical Software, Articles* **76**, 1 (2017).

[76] Stan Development Team, “PyStan: the python interface to stan, Version 2.14.0.0,” (2016).

[77] L. P. Singer and L. R. Price, *PRD* **93**, 024013 (2016).

[78] B. S. Sathyaprakash, B. F. Schutz, and C. Van Den Broeck, *Classical and Quantum Gravity* **27**, 215006 (2010).

[79] A. Nishizawa, K. Yagi, A. Taruya, and T. Tanaka, in *Journal of Physics Conference Series*, Journal of Physics Conference Series, Vol. 363 (2012) p. 012052.

[80] W. Del Pozzo, T. G. F. Li, and C. Messenger, *PRD* **95**, 043502 (2017).

[81] E. Belgacem, Y. Dirian, S. Foffa, and M. Maggiore, *PRD* **98**, 023510 (2018).

[82] S. M. Carroll, W. H. Press, and E. L. Turner, *ARA&A* **30**, 499 (1992).

[83] E. L. Wright, *PASP* **118**, 1711 (2006).

[84] T. J. Loredo, in *American Institute of Physics Conference Series*, American Institute of Physics Conference Series, Vol. 735, edited by R. Fischer, R. Preuss, and U. V. Toussaint (2004) pp. 195–206.

[85] R. L. Streit, *Poisson Point Processes* (Springer, 2010).

[86] L. Blanchet, *Living Rev. Rel.* **17**, 2 (2014).

[87] M. Maggiore, *Gravitational Waves. Vol. 1: Theory and Experiments*, Oxford Masters Series in Physics (Oxford University Press, 2007).

Appendix A: Bayesian inference of cosmological parameters from BNS mergers

The task of inferring the Hubble constant from BNS merger events can be thought of as a special case of the more general problem of cosmological parameter inference from such data (e.g., [55, 69, 80, 81]). Combined with the fact that a Euclidean approximation is insufficient even for current low-redshift BNS merger samples, taking a fully general approach and then making low-redshift approximations ensures that any such simplifications are done rigorously. The BNS merger population model (Appendix A 1), data (Appendix A 2) and sample selection (Appendix A 3) have the same structure as the more specific simulation described in Sec. IV. These ingredients are then combined self-consistently to obtain both the full posterior distribution and the marginalized posterior in the cosmological parameters (Appendix A 4).

1. Physical model

A necessary ingredient for any Bayesian inference formalism is a generative model which could be used to simulate a mock dataset. For the case of BNS mergers this includes both a cosmological model (Appendix A 1 a) and the BNS population (Appendix A 1 b), although it is primarily the structure of the model, rather than specific functional forms, which are required at this stage. This physical model includes neither measurements (Appendix A 2) or sample selection (Appendix A 3 a), which are kept distinct as they play different roles in the simulation and inference. The overall structure of the model is summarized in Fig. 8.

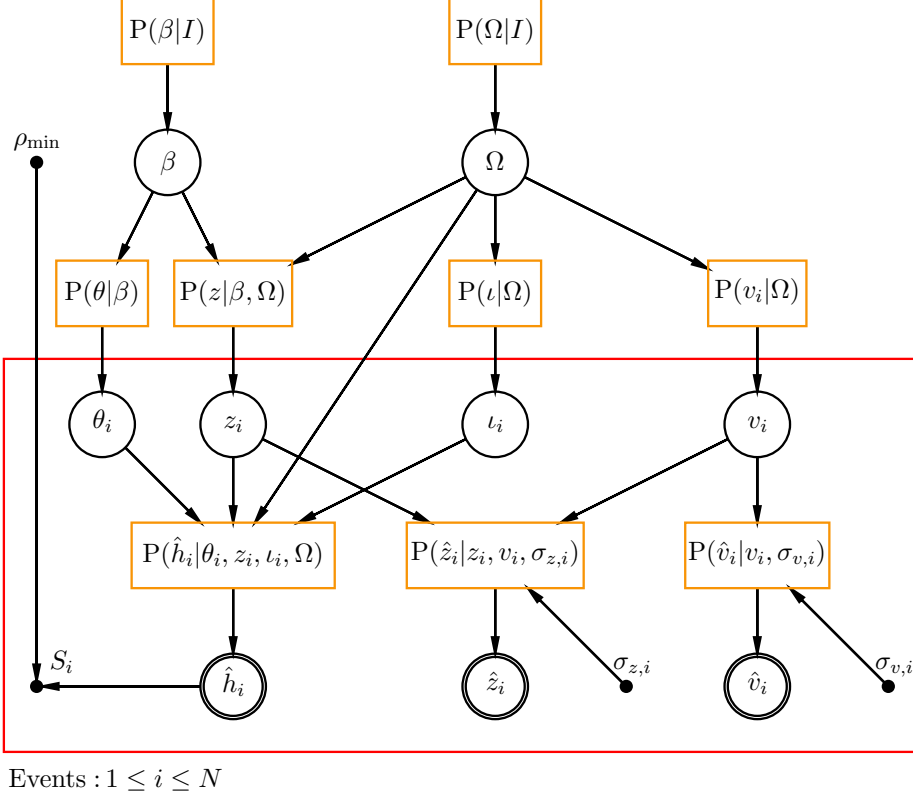


FIG. 8. Network diagram for the hierarchical model describing the BNS population and data. Quantities in single circles are model parameters; quantities in double circles are measured values. These quantities are linked by the probability distributions in orange rectangles: the top row are parameter priors; the middle row describe the population model; the bottom row define the (object-level) likelihood. The arrows linking the quantities and distributions define the forward/generative model that could be used to simulate samples and measurements. The quantities inside the red rectangular plate are specific to a single BNS merger event; the detected events are indexed by $i \in \{1, 2, \dots, N\}$.

a. Cosmology

GW signals from BNS events can, in principle, be seen to cosmological distances, and so must in general be analyzed in the context of a cosmological model. This is described by a set of parameters $\Omega = (H_0, \Omega_m, \Omega_\Lambda, \omega, \dots)$ which between them specify the contents of the universe and its expansion history. None of the results presented here depend strongly on the particular type of cosmological model adopted, so Ω is used in order to preserve generality, although it is implicit that H_0 is always included in this list.

The radial coordinate used to specify position along the line-of-sight is the (cosmological) redshift, z , defined strictly in terms of the ratio of the cosmological scale factor to the current value. This is distinct from the observable redshift, \tilde{z} , which in general differs from z due to the source's peculiar velocity relative to the Hubble-Lemaître flow. Assuming this motion is non-relativistic, the observable redshift is given in terms of the line-of-sight component of the source's peculiar velocity, v , as

$$\tilde{z} = (1 + z) \left(1 + \frac{v}{c}\right) - 1 = z + (1 + z) \frac{v}{c}, \quad (A1)$$

where positive v hence corresponds to motion away from the observer.

The redshift and cosmological model combine to specify both the the luminosity distance, $D(z, \Omega)$ and the comoving volume element $dV/dz(\Omega)$. Expressions for $D(z, \Omega)$ and $dV/dz(\Omega)$ are available for standard cosmological models [82, 83], although the model is kept general here. The numerical marginalization scheme described in Sec. IV A requires the function $z(D, \Omega)$, defined such that $z[D(z, \Omega), \Omega] = D[z(D, \Omega), \Omega] = 1$ for any cosmological model (and any non-negative value of z or D). These inverses exist in standard cosmological models as the luminosity distance increases monotonically with z [70].

b. The BNS merger population

The BNS population is defined primarily by the rate of mergers per unit proper time per unit co-moving volume, $\Gamma(z, \beta)$, where β are the parameters which specify the population model. The expected number of events in the redshift range z to $z + dz$ that would be registered by a perfect all-sky detector in time interval dt is hence

$$d\bar{N} = \frac{\Gamma(z, \beta)}{1+z} \frac{dV}{dz}(\Omega) dz dt, \quad (\text{A2})$$

where the reduction by a factor of $(1+z)$ comes about due to time dilation from the source frame, and the $dV/dz(\Omega)$ is the co-moving volume element defined in Appendix A 1 a.

The properties of a single BNS merger are separated into intrinsic system parameters, θ (the NS masses, spins, etc.), and observer-dependent quantities, which here are taken to be the inclination of the system with respect to the line-of-sight, ι , and the line-of-sight peculiar velocity of the host galaxy, v (and z , although this is already incorporated in the overall rate). For a given redshift, the population model is a (normalized) probability distribution of the form

$$P(\theta, v, \iota | z, \beta, \Omega) \propto P(\theta | z, \beta) P(v | z, \Omega) \Theta(\iota) \Theta(\pi - \iota) \frac{\sin(\iota)}{2}. \quad (\text{A3})$$

This encodes the assumption that BNS systems are oriented randomly, which leads to the sinusoidal distribution in ι .

Some care is required in treating the peculiar velocity of the BNS merger, as it has two distinct contributions: the motion of the host galaxy relative to the Hubble-Lemaître flow; and the orbital motion of the merger system within the host galaxy. (Only BNS mergers with counterparts are considered here, and all such systems have, by definition, a host galaxy.) Both these motions are expected to have typical speeds of $\sim 10^2 \text{ km s}^{-1}$, although they enter the inference formalism in distinct ways. In physical terms the peculiar velocity of the host galaxy, v , is determined by the local distribution of matter, but even in the absence of source-specific data (Appendix A 2 c), knowledge of cosmological structure formation implies a distribution of the form $P(v | z, \Omega)$. While there is a formal link between the peculiar velocity and the cosmological parameters, this is negligible compared to the link through the GW data, and so the dependence of $P(v | z, \Omega)$ on Ω can be ignored. This reflects the status of the host's peculiar velocity as a nuisance parameter in this context.

2. BNS merger data

Three distinct types of measurement provide information about the properties of a BNS merger event: GW strain time-series data (Appendix A 2 a); a spectroscopic redshift for the host galaxy (Appendix A 2 b); and, potentially, an estimated (line-of-sight) peculiar velocity for the host galaxy (Appendix A 2 c). All of these measured quantities have associated uncertainties (and other details associated with the measurement process); for brevity, all such quantities are combined into a single parameter, O , that characterizes the observations.

a. GW data

The GW signature of a merger event comprises two orthogonal polarizations, $h_p(t; \theta, \iota, v, z, \Omega)$, with $p \in \{+, \times\}$, which depend on both the intrinsic merger properties, θ , the observer-dependent quantities ι, v and z , along with the cosmological parameters, Ω . The full waveforms depend on the complicated non-linear physics of the merger, but the dependence on v and z is determined purely by the physics of GW propagation in an expanding universe. The GW signal in the far field regime is subject to a time dilation by a factor of $(1+z)(1+v/c)$ and the amplitude scales as $1/D_P(z, \Omega)$, where $D_P(z, \Omega)$ is the proper distance to redshift z , so the expression $D_P(z, \Omega) h_p[(t - t_0)/(1+z)(1+v/c), \theta, \iota, v, z, \Omega]$ is independent of redshift and peculiar velocity. The dependence of the strain on the peculiar velocity is sufficiently small that it can be ignored (Appendix B), so $h_p(t; \theta, \iota, v, z, \Omega) \rightarrow h_p(t; \theta, \iota, z, \Omega)$ is assumed.

The GW data for a merger comprise a discretized time-series of measured strains, denoted \hat{h} for simplicity, along with associated uncertainties, implicitly included in O . The likelihood for the strain data hence has the form $P(\hat{h} | \theta, \iota, z, \Omega, O)$, which is kept general in this derivation; the specific form used in the simulations described in Sec. IV is detailed in Appendix B.

b. Redshift measurement

The measured spectroscopic redshift of a BNS host, \hat{z} , is linked to both its cosmological redshift, z , and its line-of-sight peculiar velocity, v , leading to a likelihood of the form $P(\hat{z}|z, v, O)$, with the observable redshift given in Eq. A1.

c. Peculiar velocity estimates

It is possible that the (line-of-sight) peculiar velocity of a BNS host can be estimated from the positions and/or motions of nearby galaxies, yielding an estimate \hat{v} . In the absence of further information, this contribution to the likelihood has the form $P(\hat{v}|v, O)$, where the information on the positions and/or velocities of nearby galaxies is left implicit. It is unrealistic to consider the case that the uncertainty is small or negligible, as there is no credible way to get precise peculiar velocity information; but it is useful to consider the limit that the uncertainty is infinite, which is equivalent to there being no useful peculiar velocity data at all for a given system. This situation could also be recovered by removing \hat{v} and the associated likelihood from the calculation altogether.

It is also possible in principle that the line-of-sight component of the orbital motion of the merger relative to its host galaxy could be estimated (*e.g.*, through the combination of a precise location and rotation curve), although the impact of this on the GW data is minor anyway (Appendix B) so this is not explored further here.

3. Sample of BNS events

The full BNS merger dataset from a GW survey (and follow-up observations) is a catalog of N selected merger events, each with associated GW data, $\hat{h} = (\hat{h}_1, \hat{h}_2, \dots, \hat{h}_N)$ redshift measurements, $\hat{z} = (\hat{z}_1, \hat{z}_2, \dots, \hat{z}_N)$ and (possibly) host peculiar velocity information, $\hat{v} = (\hat{v}_1, \hat{v}_2, \dots, \hat{v}_N)$, as described in Appendix A 2. The additional model ingredients needed to define the sample generation process is the selection rule (Appendix A 3 a), which then determines the the number of selected events (Appendix A 3 b).

a. Selection

The selection of a BNS merger event into a sample is assumed to be determined by the GW data alone, and to take the form of a hard cut on some statistic calculated from the GW data, \hat{h} . This function is denoted $\rho(\hat{h}, O)$ and can be thought of as the observed SNR (or a proxy for this). The form of $\rho(\hat{h}, O)$ is not as important as the fact that it is deterministic, meaning the selection probability can be written as

$$P(S|\hat{h}, O) = \Theta[\rho(\hat{h}, O) - \rho_*]. \quad (\text{A4})$$

The fact that the selection is a deterministic function of the data means that for any event in a selected sample, $\rho(\hat{h}, O) \geq \rho_*$ and so $P(S|\hat{h}, O) = 1$, a critical fact [84] which simplifies the parameter inference calculation (Sec. V).

b. Number of events

Modelling the BNS merger population as a realization of a Poisson point process [85], the number of detected events in a sample is drawn from the Poisson distribution

$$P(N|\Omega, \beta, O) = \Theta(N) \frac{[\bar{N}(\beta, \Omega, O)]^N \exp[-\bar{N}(\beta, \Omega, O)]}{N!}, \quad (\text{A5})$$

which is characterized purely by the expected number of events, $\bar{N}(\beta, \Omega, O)$. This is obtained by integrating the product of the event rate and the detection probability (assumed to depend only on the GW data) over the BNS merger properties, which gives

$$\bar{N}(\beta, \Omega, O) = T \int_0^\infty dz \frac{\Gamma(z, \beta)}{1+z} \frac{dV}{dz}(\Omega) \int d\theta P(\theta|z, \beta) \int_0^\pi d\iota \frac{\sin(\iota)}{2} \int d\hat{h} P(\hat{h}|\theta, \iota, z, \Omega, O) \Theta[\rho(\hat{h}, O) - \rho_*], \quad (\text{A6})$$

where the integral with respect to t yields the observing time, T , which is included in O along with ρ_* . In general, this integral must be evaluated numerically, *e.g.*, using a Monte Carlo approach such as that described in Sec. IV F, although in some applications they can be avoided (*e.g.*, [63]).

4. Parameter inference

The general inference task here is to obtain constraints on the full set of model parameters given all the data on a sample of N BNS merger events, indexed by $i \in \{1, 2, \dots, N\}$. The full model, defined fully in Sec. IV, is characterized by the cosmological parameters, Ω , the BNS population parameters, β , and the BNS mergers' physical properties, $\boldsymbol{\theta} = (\theta_1, \theta_2, \dots, \theta_N)$, host redshifts, $\mathbf{z} = (z_1, z_2, \dots, z_N)$, and peculiar velocities, $\mathbf{v} = (v_1, v_2, \dots, v_N)$; the data for the N events are, as described in Sec. IV C, the GW measurements $\hat{\mathbf{h}} = (\hat{h}_1, \hat{h}_2, \dots, \hat{h}_N)$, redshifts measurements $\hat{\mathbf{z}} = (\hat{z}_1, \hat{z}_2, \dots, \hat{z}_N)$ and (possibly) peculiar velocity information, $\hat{\mathbf{v}} = (\hat{v}_1, \hat{v}_2, \dots, \hat{v}_N)$. Combined with a description the sample selection (Appendix A 3), this is sufficient to calculate the joint posterior distribution in all the parameters (Appendix A 4 a), and the marginalized distribution in the parameters of interest (Appendix A 4 b).

a. Joint posterior distribution

The constraints on the cosmological parameters, BNS population and the individual events implied by a sample of N detected BNS mergers are fully described by the joint posterior distribution in all the model parameters, $P(\boldsymbol{\theta}, \boldsymbol{\iota}, \mathbf{z}, \mathbf{v}, \beta, \Omega | N, \hat{\mathbf{h}}, \hat{\mathbf{z}}, \hat{\mathbf{v}}, O, I)$, where I is the prior information assumed about Ω and β . The knowledge about the cosmological model and the BNS population are assumed to be independent, so that the prior factorizes as $P(\Omega, \beta | I) = P(\Omega | I) P(\beta | I)$; the prior information on all the other parameters is specified by Ω and β , and so is conditionally-independent of I . The posterior is conditioned not only on the obvious data for each of the merger events (*i.e.*, $\hat{\mathbf{h}}$, $\hat{\mathbf{z}}$ and $\hat{\mathbf{v}}$), but also on the size of the sample (*i.e.*, the value of N) and hence implicitly on the fact that the GW data from each event satisfies the selection criterion outlined in Appendix A 3 a.

The task now is to write the joint posterior distribution in terms of the functions/distributions defined in Appendix A 1, Appendix A 2 and Appendix A 3. It is useful to introduce explicitly the fact that each of the merger events was selected, denoted $\mathbf{S} = (S_1, S_2, \dots, S_N)$ following Appendix A 3 a. This can be added to the list of quantities being conditioned on because the selection process defined in Eq. 21 is deterministic – whether \mathbf{S} is true can be determined from \hat{h} – which means that including \mathbf{S} does not add any extra information: $P(\boldsymbol{\theta}, \boldsymbol{\iota}, \mathbf{z}, \mathbf{v}, \beta, \Omega | N, \hat{\mathbf{h}}, \hat{\mathbf{z}}, \hat{\mathbf{v}}, O, I) = P(\boldsymbol{\theta}, \boldsymbol{\iota}, \mathbf{z}, \mathbf{v}, \beta, \Omega | N, \mathbf{S}, \hat{\mathbf{h}}, \hat{\mathbf{z}}, \hat{\mathbf{v}}, O, I)$. The reason for including \mathbf{S} is that it gives the freedom to condition on selection alone, which allows the the unnormalized posterior to be written as

$$P(\boldsymbol{\theta}, \boldsymbol{\iota}, \mathbf{z}, \mathbf{v}, \beta, \Omega | N, \hat{\mathbf{h}}, \hat{\mathbf{z}}, \hat{\mathbf{v}}, O, I) \propto P(\Omega | I) P(\beta | I) P(N | \Omega, \beta, O) \prod_{i=1}^N P(\theta_i, \iota_i, z_i, v_i, \hat{h}_i, \hat{z}_i, \hat{v}_i | S_i, \beta, \Omega, O). \quad (\text{A7})$$

The first two terms are the prior distributions on the cosmological and BNS population parameters; the second term encodes the constraints provided by the number of detected events (Sec. IV E); but the terms in the product still require some manipulation to be written in terms of the distributions which define the model. Taking any one such term and successively applying Bayes's theorem, the chain rule, and the law of total probability then yields the joint distribution in the intrinsic and observed properties of a selected merger event as

$$P(\theta, \iota, z, v, \hat{h}, \hat{z}, \hat{v} | S, \beta, \Omega, O) \quad (\text{A8})$$

$$= \frac{1}{\bar{N}(\Omega, \beta, O)} \frac{\Gamma(z, \beta)}{1+z} \frac{dV}{dz}(\Omega) P(\theta | z, \beta) \Theta(\iota) \Theta(\pi - \iota) \frac{\sin(\iota)}{2} P(v | z, \Omega) P(\hat{h} | \theta, \iota, z, \Omega, O) P(\hat{z} | z, v, O) P(\hat{v} | v, O),$$

where the fact that $P(S | \hat{h}, O) = 1$ for selected events has been used to omit this term, and the normalizing constant is equal to the expected number of events in the sample, given in Eq. A6.

Inserting this object-level distribution and the Poisson distribution of the number of events in Eq. A5 into Eq. A7 then gives the unnormalized joint posterior distribution in all the model parameters as

$$P(\boldsymbol{\theta}, \boldsymbol{\iota}, \mathbf{z}, \mathbf{v}, \beta, \Omega | N, \hat{\mathbf{h}}, \hat{\mathbf{z}}, \hat{\mathbf{v}}, O, I) \propto P(\Omega | I) P(\beta | I) \exp[-\bar{N}(\beta, \Omega, O)] \quad (\text{A9})$$

$$\times \prod_{i=1}^N \frac{\Gamma(z_i, \beta)}{1+z_i} \frac{dV}{dz_i}(\Omega) \Theta(\iota_i) \Theta(\pi - \iota_i) \sin(\iota_i) P(\theta_i | z_i, \beta) P(\hat{h}_i | \theta_i, \iota_i, z_i, \Omega, O) P(v_i | z_i, \Omega) P(\hat{z}_i | z_i, v_i, O) P(\hat{v}_i | v_i, O),$$

where the selection indicators \mathbf{S} have been omitted because (as argued above) they do not contain any extra information beyond that already encoded in $\hat{\mathbf{h}}$. This has the standard structure for the full likelihood of a Poisson point process [85], in particular with the expected number of detected sources appearing only in the exponential term, although the number of different component distributions in the product somewhat obscures the link to this

standard statistical model. This posterior has the characteristic Poisson point process structure that also appears in *e.g.*, Refs. [63, 66].

Equation A9 represents the main result of the above model formulation as it encodes all the links between the measured data and the quantities of interest. Other than the assumption of random orientations encoded in the sinusoidal inclination distribution, it is deliberately kept completely general, with only the structure of the conditional dependencies from Fig. 8 enforced. Importantly, this result is valid in a fully cosmological context, which means it also provides a rigorous route to obtaining low-redshift approximations without the need for any heuristic arguments about the relationship between distance, redshift and line-of-sight velocity.

b. Marginalization over nuisance parameters

The main scientific aim here is inference of the cosmological parameters, and specifically H_0 , which casts all the individual and population-level BNS quantities as nuisance parameters to be integrated out. For the simple model described in Sec. IV this is done by sampling the joint posterior distribution, as described in Sec. V, and so there is no need to explicitly calculate the marginalized posterior distribution. The alternative approach [46, 53, 54], which will likely be needed when analyzing real data, is to separately marginalize over the redshift parameters constrained by the EM data and then use samples from the individual merger posteriors to marginalize over those parameters. Equation A9 can be used as the basis for this approach, with the only potential difference coming from how the pre-factor of $\exp[-\bar{N}(\beta, \Omega, O)]$ is handled. Fortunately, this term has only a weak dependence on H_0 for low-redshift samples ([46, 53] and Sec. IV E), so such choices should not strongly affect the final marginal posterior distribution in Ω .

Appendix B: Likelihood for the merger inspiral

A BNS merger is driven by non-linear physics in dynamical strongly curved spacetime, and hence described by a large number of parameters. But within the frequency band of the current GW detectors the signals relevant for distance constraints arise primarily from the comparatively simple inspiral phase preceding the merger, which can be modeled using the post-Newtonian approximation in general relativity *e.g.*, [86]. The only relevant physical and geometric source parameters at Newtonian order are: the redshift, z ; the chirp mass, $\mathcal{M} = (M_1 M_2)^{3/5}/(M_1 + M_2)^{1/5}$, where M_1 and M_2 are the masses of the two NSs; the GW polarization angle, the luminosity distance, the sky position and the inclination to the line-of-sight, ι . For simplicity, it is assumed that the spins of the NSs are zero, which is consistent with the known extremely low spins (< 0.04 for their dimensionless spins) of Galactic BNSs that will merge within a Hubble time [49]. Adopting these simplifications, the GW signal from a merger event takes the form of two orthogonal strain waveforms. To leading order in the post-Newtonian expansion parameter these can be written as (*e.g.*, [87])

$$h_+(t) = \frac{G \mathcal{M}/c^2}{D_P(z, \Omega)} \frac{1 + \cos^2(\iota)}{2} \phi_+ \left[t; \frac{5G}{c^3} (1+z) \left(1 + \frac{u}{c} + \frac{v}{c}\right) \mathcal{M}, t_c, \Phi_c \right] \quad (B1)$$

$$h_\times(t) = \frac{G \mathcal{M}/c^2}{D_P(z, \Omega)} [-\cos(\iota)] \phi_\times \left[t; \frac{5G}{c^3} (1+z) \left(1 + \frac{u}{c} + \frac{v}{c}\right) \mathcal{M}, t_c, \Phi_c \right],$$

where the time-dependence is encoded in

$$\phi_+(t; \tau, t_c, \Phi_c) = \left(\frac{t_c - t}{\tau} \right)^{-1/4} \cos \left\{ 2 \left[\Phi_c - \left(\frac{t_c - t}{\tau} \right)^{5/8} \right] \right\} \quad (B2)$$

$$\phi_\times(t; t_c, \tau, \Phi_c) = \left(\frac{t_c - t}{\tau} \right)^{-1/4} \sin \left\{ 2 \left[\Phi_c - \left(\frac{t_c - t}{\tau} \right)^{5/8} \right] \right\},$$

and where t_c is the detector-frame time of coalescence, Φ_c is the orbital phase at this time, ι is the inclination of the system relative to the line-of-sight, z is the (cosmological) redshift of the system, v is the (line-of-sight) peculiar velocity of the host galaxy, u is the (line-of-sight) velocity of the merger relative to the host, and Ω are the cosmological parameters, with $D_P(z, \Omega)$ the proper distance to redshift z .

The observer frame coalescence time-scale, τ , is proportional to the intrinsic orbital period, which scales as $\sim G\mathcal{M}/c^3$, but is also subject to a time-dilation. Ignoring gravitational redshifting effects and assuming both the peculiar velocity of the host galaxy and the motion of the BNS system relative to it are non-relativistic, this is given by $\sim (1+z)(1+u/c+v/c)$. Any measurement of τ can hence only provide constraints on the redshifted chirp mass, $\hat{\mathcal{M}}_z = (1+z)(1+u/c+v/c)\mathcal{M}$.

The GW data from a single detector is a single time-series of measured strains, given by a linear combination of the orthogonal strain waveforms given in Eq. B1 that depends on the detector's orientation, along with associated uncertainties and correlations. With multiple detectors it is possible to extract information about both polarizations (*e.g.*, [87]). For a well-measured event, like GW 170807, the oscillatory nature of the several thousand cycles of the inspiral signal allows precise constraints to be placed on the parameters τ , t_c and Φ_c that determine the time-dependence according to Eq. B2; the measured amplitudes then place largely independent, if more uncertain, constraints on the amplitudes of the two strain waveforms. The parameter-dependence of the likelihood can hence be captured by reducing the full dataset to a small set of (nearly) sufficient statistics that can be calculated from the data: the accurately measured coalescence time, \hat{t}_c ; the accurately measured coalescence phase, $\hat{\Phi}_c$; the accurately measured time-scale, $\hat{\tau}$; and noisy estimates of the two orthogonal amplitudes, \hat{A}_+ and \hat{A}_\times , which are both taken here to have (the same) uncertainty, σ_A . This is an unrealistic simplification, as shown by the sample variance seen in Ref. [54] and discussed at length by Ref. [53]. It is convenient to convert from $\hat{\tau}$ to the measured redshifted chirp mass, defined as $\hat{\mathcal{M}}_z = \hat{\tau}/(5G/c^2)$. Assuming no uncertainty on the temporal parameters, and Gaussian noise on the amplitudes, the GW likelihood can be approximated as

$$\begin{aligned} & P(\hat{t}_c, \hat{\Phi}_c, \hat{\mathcal{M}}_z, \hat{A}_+, \hat{A}_\times | \mathcal{M}, t_c, \Phi_c, \iota, z, u, v, \Omega) \\ &= \delta(\hat{t}_c - t_c) \delta(\hat{\Phi}_c - \Phi_c) \delta\left[\hat{\mathcal{M}}_z - (1+z)\left(1 + \frac{u}{c} + \frac{v}{c}\right)\mathcal{M}\right] N\left[\hat{A}_+; \frac{G\mathcal{M}/c^2}{D_P(z, \Omega)} \frac{1 + \cos^2(\iota)}{2}, \sigma_A^2\right] N\left[\hat{A}_\times; -\frac{G\mathcal{M}/c^2}{D_P(z, \Omega)} \cos(\iota), \sigma_A^2\right] \\ &= \delta(t_c - \hat{t}_c) \delta(\Phi_c - \hat{\Phi}_c) \frac{\delta[\mathcal{M} - \hat{\mathcal{M}}_z/(1+z)(1+u/c+v/c)]}{(1+z)(1+u/c+v/c)} \\ &\quad \times N\left[\frac{G\hat{\mathcal{M}}_z/c^2}{(1+u/c+v/c)D(z, \Omega)} \frac{1 + \cos^2(\iota)}{2}; \hat{A}_+, \sigma_A^2\right] N\left[-\frac{G\hat{\mathcal{M}}_z/c^2}{(1+u/c+v/c)D(z, \Omega)} \cos(\iota); \hat{A}_\times, \sigma_A^2\right], \end{aligned} \quad (B3)$$

where the second form of the likelihood exploits the tight constraint on the redshifted chirp mass to remove \mathcal{M} from the two amplitude terms, and $D(z, \Omega) = (1+z)D_P(z, \Omega)$ is the luminosity distance.

Once the time-dependence of the observed waveform has been used to constrain $\hat{\mathcal{M}}_z$, the measured amplitudes provide direct constraints on a combination of the ι and $D(z, \Omega)$, with the peculiar velocity terms producing a negligible relative offset of $\lesssim 1\%$. As such it is reasonable to ignore them completely (*i.e.*, effectively setting $u = v = 0$), although it is interesting to note that the dependence on v is such that there is a small cancellation with the error induced by the host's peculiar velocity on the measured redshift that is almost exact (if unimportant) at $z \simeq 1$. The coalescence time and phase can similarly be ignored, leaving the significant part of the likelihood as

$$\begin{aligned} & P(\hat{\mathcal{M}}_z, \hat{A}_+, \hat{A}_\times | \mathcal{M}, \iota, z, \Omega, O) \\ &= \delta\left[\hat{\mathcal{M}}_z - (1+z)\mathcal{M}\right] N\left[\hat{A}_+; \frac{G(1+z)\mathcal{M}/c^2}{D(z, \Omega)} \frac{1 + \cos^2(\iota)}{2}, \sigma_A^2\right] N\left[\hat{A}_\times; -\frac{G(1+z)\mathcal{M}/c^2}{D(z, \Omega)} \cos(\iota), \sigma_A^2\right] \end{aligned} \quad (B4)$$

This form of the likelihood is used in Sec. IV C.